Ocean Engineering 63 (2013) 77–89

Contents lists available at SciVerse ScienceDirect

Ocean Engineering

journal homepage: www.elsevier.com/locate/oceaneng

Refraction and diffraction of water waves using finite elements with a DNL boundary condition

Ruperto P. Bonet Chaple*

Department of Mathematics, National University of San Luis, Chacabuco y Pedernera, 5700 San Luis, Argentina

ARTICLE INFO

Article history:
Received 21 September 2011
Accepted 6 October 2012
Available online 21 March 2013

Keywords:
Absorbing boundary condition
Helmholtz
Diffraction
Refraction
Water waves

ABSTRACT

A discrete non-local (*DNL*) boundary condition is used to solve diffraction and refraction water waves problems. The finite elements with a *DNL* boundary condition are used to solve a wide range of unbounded surface wave problems. Two order low strategies are examined in rectangular and/or circular two-dimensional coordinates system. Numerical studies reveal the advantages of using this numerical approach and its limitations in case of variations of wave number in direction to infinity. Two new procedures to improve the accuracy of *DNL* boundary in case of significant variations of wave number in the domain are therefore developed. These procedures are based on the addition of a term to the numerical scheme, that collects the error away from the open boundary. Such term can be incorporated into the *DNL* formula as a source term or as an additional layer. This improvement permits the development of a suitable solution method, which is tested against analytical solutions and other methods, for bi-dimensional water waves problems defined on rectangular or circular geometries. Also, implementation details are reported. Satisfactory numerical results confirm the improvement of *DNL* method in case of dependent range, which allow us to conclude that the *DNL* method is an achievable method for the solution of unbounded water waves problems governed by the Helmholtz equation.

1. Introduction

The water waves general problem considered allows us to describe the pattern of surface waves originated when plane monochromatic waves travelling through a fluid of constant depth encounter an area of varying depth and obstacles. The model equation used to describe this problem is Berkhoff's equation, which is based on a potential representation of the velocities in the fluid with a linearized surface boundary condition for a bottom with a mild slope. This two-dimensional equation must be solved in a domain which is assumed unbounded and infinite. The presence of obstacles, or islands within the domain causes radiation of the waves to infinity and the mathematical model of the system must be able to deal with this. The present approach is to model the entire domain using finite elements on a given bounded region and the *DNL* method on an unbounded domain.

A significant amount of research has been done in the development of techniques to model water waves problems in unbounded domain adequately, and a significant number of mathematical techniques are in use. The *DtN* method is a analytical procedure introduced and applied to time-harmonic wave problems (Givoli and Keller, 1989; Givoli, 1991, 1992a, 1992b) and extended for acoustic problems in Harari and Hughes (1994) and Harari et al. (1998). This boundary condition is exact and non-reflecting, but the basis system must be selected according to the space dimension of the problem at hand, and in virtue of the truncated *DtN* map is no-local in space, in the finite element framework, the resulting system of linear equations is not sparse.

Others methods, based on cloning type algorithms, have been developed (Dasgupta, 1981; Wolf and Song, 1996). The consistent infinitesimal finite-element cell method is used to model the unbounded medium for the scalar and vector wave equation elastodynamics and diffusion in frequency and time domains. This method is a boundary finite-element procedure, which is exact in the finite-element sense, and after taking the limit of the infinitesimal cell width, the unbounded domain is cloned.

As an alternative to the *DtN* method, a discrete non-local *DNL* formulation for a finite element method on an unbounded domain in water waves propagation problems is presented (Bonet et al., 1997; Storti et al., 1998). This formulation is based on finding the general solution of a recurrence relationship involving the complete eigen-decomposition of the resulting difference operator by *FEM* or *FDM*. To close the computational domain uses a structured mesh with quadrangular linear elements as in Thatcher (1976, 1978). The planar *DNL* boundary condition is non-local in space (as well as, truncated *DtN* map), non-reflective and exact at discrete level.

Firstly, the present paper includes a review of the description of the *DNL* method in rectangular coordinates and/or circumferential coordinates. Secondly, a numerical study to reveal the performance of this methodology is presented, and finally, an extension of it

* Tel.: +54 2652 42 67 59; fax: +54 2652 44 40 14.
E-mail address: rpbonet@unsl.edu.ar

0029-8018/$ - see front matter © 2012 Elsevier Ltd. All rights reserved.
http://dx.doi.org/10.1016/j.oceaneng.2012.10.006

including a higher order difference scheme is reported. Numerical solutions for several water waves problems are obtained by means of application of finite elements with a *DNL* boundary condition, such waves diffracted around a cylinder, waves refracted by a parabolic shoal with a cylinder on top, and waves in a rectangular harbor, among others.

2. Theory

The theory presented here is based on the formulation of the velocity potential ϕ (a time harmonic function according to the $e^{i\omega t}$ law). This model equation describes adequately the propagation of long and short waves over a bottom of mild slope. We consider the two-dimensional Berkhoff equation with wave number k (Berkhoff, 1976)

$$\nabla_h(CC_g\nabla\phi)+k^2CC_g\phi=0 \tag{1}$$

in an unbounded domain, with the scattered field $\phi=\phi^s$ satisfying the Sommerfeld radiation condition at infinity (Harari and Hughes, 1994). Here ∇ is the horizontal gradient operator, ω is the angular frequency, g is the gravitational acceleration, and $h=h(x,y)$ is the water depth. C and C_g are the phase and group velocity, respectively; $k=\omega/C\geq 0$ is the wave number; such that $k(x,y)$ changes continuously reaching the constant k_0 value at the outer part of any bounded and closed region.

2.1. Finite elements in an unbounded domain

The *DNL* procedure solves the two-dimensional discrete Helmholtz equation (Berkhoff equation with a constant k_0 refraction index) in an unbounded domain, over a patch around the computational domain, using numerical scheme on a structured mesh.

Fig. 1 shows the discretization employed over a structured mesh in case of rectangular geometry. In the direction to infinity three successive layers $j-1$, j, $j+1$ are represented. On each layer there are N_{lay} nodes equispaced, therefore, the mesh has N_{lay} nodes in the transversal direction.

By means of the finite difference method (*FDM*) or the finite element method (*FEM*) applied to a structured grid, the discrete Helmholtz equation for the layer j can be given as

$$\mathbf{C}^j\phi^{j-1}+\mathbf{B}^j\phi^j+\mathbf{A}^j\phi^{j+1}=0 \tag{2}$$

where ϕ^j is the vector containing scattered potential values for the nodes belonging to the j layer. In the circular or spherical boundary cases the $\mathbf{A}^j$,$\mathbf{B}^j$ and $\mathbf{C}^j$ matrices at successive layers are different, due to the r^j factors, in contrast to the rectangular geometry, which is only dependent of wave number k_0 and the discretization step h. In the latest case, the $\mathbf{C}^j$ and $\mathbf{A}^j$ matrices are the same.

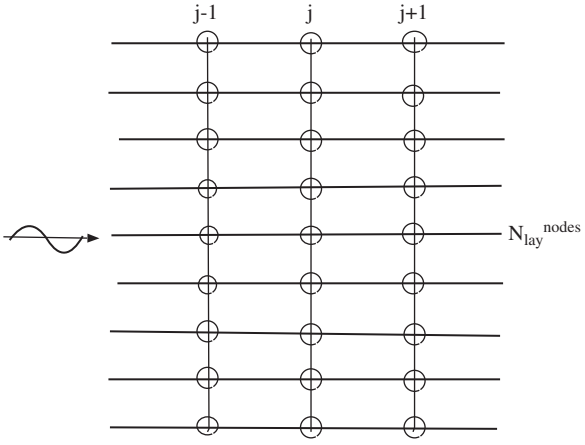

Fig. 1. Discretization on a structured mesh in rectangular coordinates.

For rectangular geometry Eq. (2) can be expressed in the form

$$L(\mu)=\mu^2\mathbf{I}+\mu\mathbf{\Lambda}+\mathbf{I}=(\mu^+\mathbf{I}-\mathbf{G})(\mu^-\mathbf{I}-\mathbf{H}) \tag{3}$$

where $(\mathbf{A}^j)^{-1}\mathbf{B}^j=\mathbf{V}\mathbf{\Lambda}\mathbf{V}^{-1}$. Here $\mathbf{V}$ and Λ are the corresponding eigenvector and eigenvalue matrices, respectively. Factorizating (3) the wave-field can be splitted into "forward modes" and the "backward modes", corresponding to μ^+ and μ^- values, respectively. These values were characterized in Bonet et al. (1998, 1999a, 1999b). In virtue of this, we can express the non-local relation

$$(\phi^+)^{j+1}=\mathbf{F}^j(\phi^+)^j \tag{4}$$

where $\mathbf{F}^j=\mathbf{F}=\mathbf{VGV}^{-1}$ for each j-layer. The $\mathbf{F}$ matrix is called "planar *DNL* matrix".

The circumferential *DNL* procedure is based on the full solution of the exterior problem governed by the discretized Helmholtz operator with constant refraction index. For this, the unbounded domain (see Fig. 2) is subdivided into two parts, a bounded region (the annular region $r_i\leq r\leq r_e$, $-\pi\leq\theta\leq\pi$ and an unbounded semi-infinite region (the region $r\geq r_e$). Fig. 2 (left) shows the scatterers surrounded by a circle of radius r_i, located at the artificial boundary (in the near field) and the successive circles(o layers) until the circle $r=r_e$ (in the far field), which is taken sufficiently large such that the influence of curvature can be neglected.

Due to r-dependence, the $\mathbf{F}^j=\mathbf{F}$ equality does not yield for all j-layers, then the derivation of the *DNL* method in the near field is obtained by means of the recursive process of calculus from the far-field ($j=M$) to the near field ($j=1$) (see Fig. 2 (right)). Eq. (4) is used at the far-field (for $r=r_e$ sufficiently large) and by means of the recursive relation

$$\mathbf{F}^{j-1}=-(\mathbf{A}^j\mathbf{F}^j+\mathbf{B}^j)^{-1}\mathbf{C}^j \tag{5}$$

from layer $j=M$ to $j=2$, is obtained the *DNL* matrix at the near field $r=r_i$, and the relation

$$(\phi^+)^2=\mathbf{F}^1(\phi^+)^1 \tag{6}$$

on the artificial boundary $r=r_i$. This relation in the near field represents a discrete non-local solution of the exterior problem governed by the Helmholtz equation. We recall the attention relative to the $\mathbf{F}^1$ matrix containing all the information on the behaviour of the scattered wave field from the far-field. This process is numerically stable, and it's named 'condensation from the plane *DNL* matrix to the circular *DNL* matrix'.

2.2. Effectiveness of the DNL absorbing boundary condition

The following analysis evaluates the $kh(kr)$-dependence of the performance of DNL absorbing boundary condition specified on an open boundary Γ that bounds a computational domain Ω, which is discretized by finite elements. A measure of the effectiveness of absorbing boundary conditions for acoustic wave problems is investigated in Harari (2004) using the following exact specific impedance:

$$z(x)=\frac{ik\phi}{\dfrac{\partial\phi}{\partial\mathbf{n}}} \tag{7}$$

Employing a low order scheme, we obtain a discrete version of (7)

$$z^h(x)=\frac{ikh\phi^j}{\phi^{j+1}-\phi^j} \tag{8}$$

to evaluate the performance of *DNL* absorbing boundary condition, in rectangular and/or circumferential coordinates. The precision in

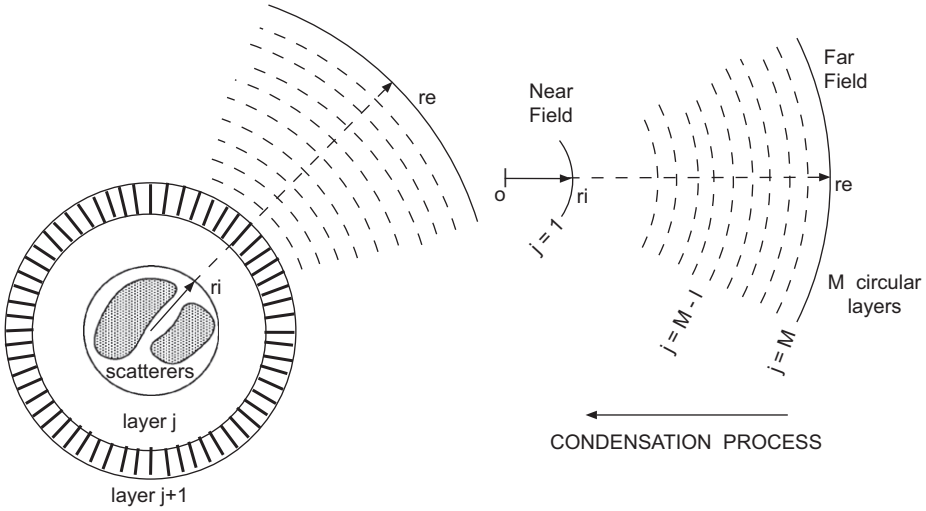

Fig. 2. Circular *DNL* method (left). Sketch on the scattering process by *DNL* method (right). Condensation process.

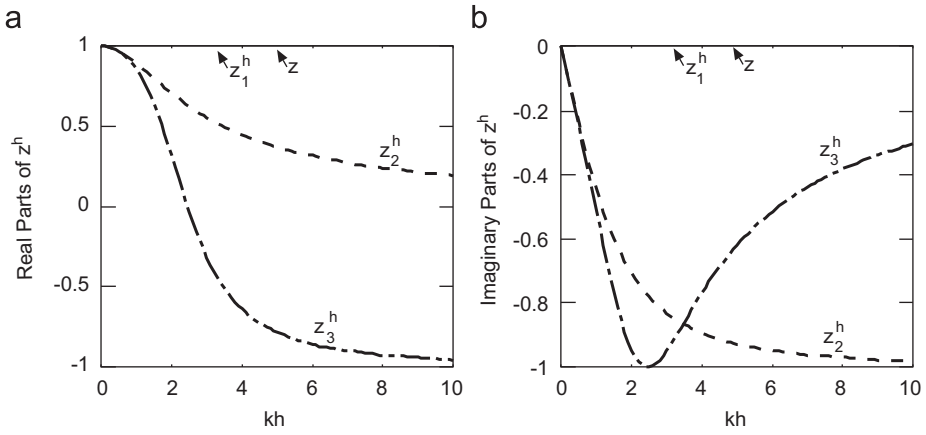

Fig. 3. Discrete specific impedance for the planar *DNL* boundary condition: (a) Real parts of z_m^h and (b) imaginary parts of z_m^h, $m=1, 2, 3$.

which a discrete absorbing boundary condition represents the unbounded medium may be assessed by comparing its specific impedance $z^h(x)$ for given problems to exact values $z(x)$ at various frequency regimes.

2.2.1. Waves propagation in a semi-infinite rectangular channel of constant depth

We consider a problem of water waves propagation in a rectangular channel of constant depth and rigid walls. A coordinates system associated to this problem indicates the x-axis in the longitudinal direction and the y-axis in the transversal direction (see Fig. 1). For a plane wave of amplitude 1 that incides from the left side, an exact solution to this problem can be given by the formula

$$\phi^e = e^{i\sqrt{k^2-(n\pi/L)^2}x}\cos\left(\frac{n\pi y}{L}\right) \tag{9}$$

where L is the length of the transversal section of the channel and n-indicates the transversal modes order. For normal incidence is excited the principal mode, that is, for $n=0$. The exact values of the specific impedance $z(x)$ are computed substituting the formula (9) into Eq. (7), and then, leads

$$z(x) = \frac{k}{\sqrt{k^2-\left(\frac{n\pi}{L}\right)^2}} \tag{10}$$

which is equal to 1 in case of normal incidence ($n=0$). The values of the discrete specific impedance $z^h(x)$ are computed using the discrete equation of Helmholtz equation (2), in which the corresponding n-modal equation can be written in the following manner:

$$\phi^{j-1}-(2-(lh)^2)\phi^j+\phi^{j+1}=0 \tag{11}$$

where $l=\sqrt{k^2-(n\pi/L)^2}$. Considering the approximations $\cos(lh)=1-(lh)^2/2$, and $\phi^{j+1}=\mu\phi^j$ Eq. (11) can be transformed to the quadratic equation

$$\mu^2-2\cos(lh)\mu+1=0 \tag{12}$$

where $e^{\pm ilh}$ are its solutions. Taking $\mu=e^{ilh}$ we get the relations

$$\phi^{j+1}=e^{ilh}\phi^j \tag{13}$$

and

$$z^h(x)=\frac{ikh}{e^{ilh}-1}=\frac{ikh}{e^{i\sqrt{(kh)^2-(n\pi h/L)^2}}-1} \tag{14}$$

The formula (14) allows us to compute the discrete specific impedance of *DNL* absorbing boundary condition for the water waves problem in a rectangular channel of constant depth. Using a lower order approximation, $z^h(x)\equiv z(x)$ for all n values, and therefore, the discrete specific impedance given in (14) is exact for a low order scheme. Using approximations to e^{ilh} of order 1, 2 and 3 for $n=0$, we get the discrete specific impedances $z_m^h(x)$, $m=1, 2, 3$ written in the following manner:

$$z_1^h(x)=1 \tag{15}$$

$$z_2^h(x) = \frac{1}{1+\frac{ikh}{2}} \tag{16}$$

$$z_3^h(x) = \frac{1}{1+\frac{ikh}{2}-\frac{(kh)^2}{6}} \tag{17}$$

Fig. 3 displays the real and imaginary parts of $z_m^h(x)$ in case of normal incidence. Also we can appreciate the lost of accuracy of the discrete specific impedance when the numerical boundary fluxes are computed using higher order schemes, and it is more noticeable as the frequency increases. This behavior is probably due to the integration of the discrete equations at the interior od the computational domain with a low order scheme.

2.2.2. Scattering of a plane wave by a circular island

Consider an incident plane wave along the positive x-axis

$$\phi^i = \exp(ikx) \tag{18}$$

scattered by a circular island of radius a. The angle to the direction of the incident wave is $\theta = \arctan(y/x)$, so that there is no restriction in this choice of direction. Due to the hard boundary condition imposed on the island ($r=a$), the scattered field can be obtained from the series representation in the following manner (Berkhoff, 1976):

$$\phi(r,\theta) = -2\sum_{n=0}^{\infty}{}' i^n \frac{J_n'(ka)H_n^{(1)}(kr)}{H_n^{(1)'}(ka)}\cos(n\theta) \tag{19}$$

where the prime on the sum indicates that the first term is halved. The derivative on the boundary $r=2a$ is

$$\frac{\partial\phi}{\partial r}(2a,\theta) = -2k\sum_{n=0}^{\infty}{}' i^n \frac{J_n'(ka)H_n^{(1)'}(2ka)}{H_n^{(1)'}(ka)}\cos(n\theta) \tag{20}$$

The exact specific impedance of the scattered field on the boundary is then obtained using equation (7). One can observe that the result depends on ka and on the angle (from the incident plane wave) θ.

The asymptotic values of the discrete specific impedance $z^h(x)$ are computed based on the discretization of the Helmholtz equation in polar coordinates

$$\frac{\partial^2\phi}{\partial r^2}+\frac{1}{r}\frac{\partial\phi}{\partial r}+\frac{1}{r^2}\frac{\partial^2\phi}{\partial\theta^2}+k^2\phi = 0 \tag{21}$$

in which the corresponding n-modal equation adopts the form

$$\frac{\partial^2\psi}{\partial r^2}+\left(k^2+\frac{1-4n^2}{4r^2}\right)\psi = 0 \tag{22}$$

using the transformation $\psi = \sqrt{r}\phi$. The discrete equation of low order corresponding to (22) can be written as follow

$$\psi^{j-1}-(2-(l^j h)^2)\psi^j+\psi^{j+1} = 0 \tag{23}$$

where $l^j = \sqrt{k^2+1/4r^{j2}-(n/r^j)^2}$. Following steps (11)–(13) we can get an asymptotic formula for specific impedance as ($kr \gg 1$)

$$z^h(r^j) = \frac{ikh}{\left(\frac{\sqrt{r^j}}{\sqrt{r^{j+1}}}\right)(e^{il^j h}-1)} = \approx \frac{\sqrt{r^{j+1}}}{\sqrt{r^j}\sqrt{1+\frac{1}{4(kr^j)^2}-\left(\frac{n}{kr^j}\right)^2}} \tag{24}$$

Fig. 4 displays the curves corresponding to the real and imaginary parts of specific impedances Z and Z^h in case of circumferential coordinates. Asymptotic expression to Z^h of low order has an excellent behaviour as $kr \gg 1$, as we can expected. A more detailed analysis of the effectiveness of the circular *DNL* method is shown in Fig. 5 along of the open boundary. Fig. 5 displays the measures $E_{2,r} = \|Real(\phi^{j+1}-F^j\phi^j)\|_2/ka$ and $E_{2,i} = \|Imag(\phi^{j+1}-F^j\phi^j)\|_2/ka$ as $0 < ka \ll 10$. We can appreciate that the precision is deteriorated as ka takes values close to zero, while the precision increases as ka

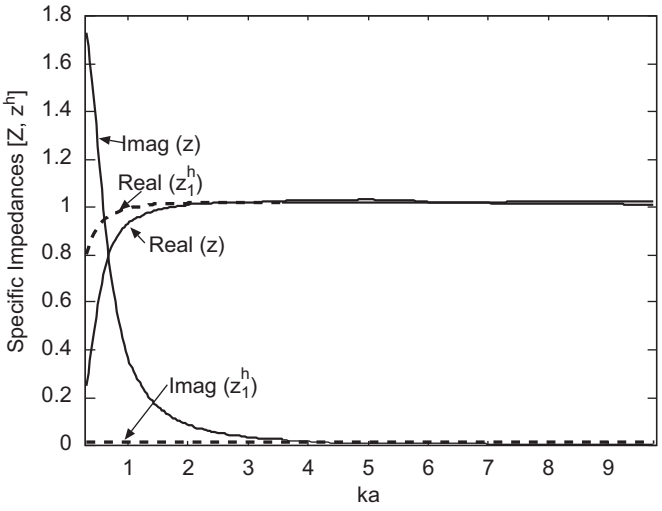

Fig. 4. Specific impedances for the circular *DNL* boundary condition. Analytical impedance z. Asymptotic approximation z_1^h for $n=0$.

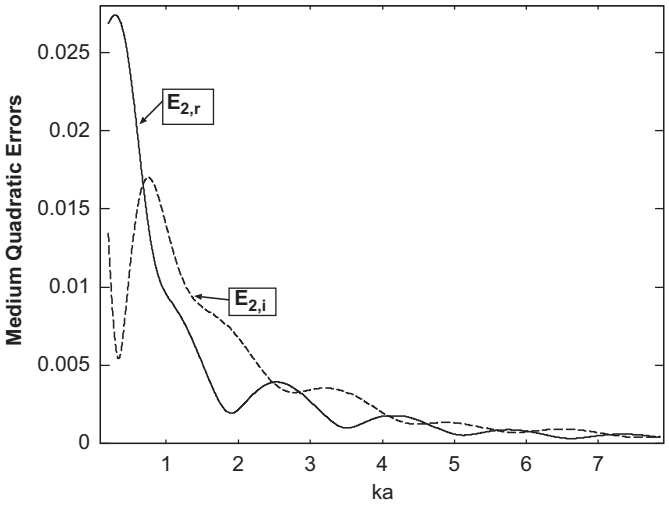

Fig. 5. Medium quadratic errors normalized $E_{2,r}$ and $E_{2,i}$.

wave numbers increases. Also, we can appreciate that both measures $E_{2,r}$ and $E_{2,i}$ decrease in oscilant form as ka increases, and these have an stable behaviour as $kr \gg 1$, that is corresponding to the results shown in Fig. 4 employing asymptotic expressions of the specific impedance Z^h.

An exhaustive evaluation of the performance of the circular *DNL* boundary condition in all frequency regimes is shown in Section 2.3.2 computing the medium quadratic error E_2 (see formula (25)).

2.3. Numerical studies

Next we want to investigate the effects of discretization on the *DNL* boundary condition. First, we study the convergence of numerical solution by *DNL* method when the discretization step h approximates to zero. Second, we notice some aspects relative to the computational implementation and its advantages and limitations.

2.3.1. Convergence

We study the convergence process the numerical solution obtained by *DNL* method relative to the element size h^2, employing

structured meshes with a resolution of 10, 20, 30 and 40 elements by wavelength (e/λ). We wish to show that the planar *DNL* boundary condition converges to perfectly absorbing boundary condition in the continuum medium when h goes to zero. Errors for several incidence angles $\theta(k_y/k=\sin(\theta))$ are computed putting the exact solution $\phi_l^j=\exp i(k_y h_y l+\sqrt{k^2-k_y^2}h_x j)$, $l=1,2,\ldots,N_{lay}$ into the formula (4). Fig. 6 displays the absolute values of phase errors ($|\sigma|$) using semilogarithmic plots. We can appreciate that the ($|\sigma|$) values uniformly decrease as the element size decreases, and then, the phase error succession is convergent to zero when h approximates to zero. Also, as we expected, the maximum error on each curve is reached for an incidence angle close to 90°.

2.3.2. Numerical implementation details

In this section we describe the main aspects in the numerical implementation of the *DNL* method, which allow a better computational performance in the application of this method.

The planar *DNL* procedure is based on the eigenvalue decomposition of the global matrices $\mathbf{C}^j,\mathbf{B}^j,\mathbf{A}^j$ which are obtained to solve the discrete Helmholtz equation in Eq. (2). In this case, due to the symmetry of this matrices the computing of the *DNL* matrix can be done at the eigenbasis system easily.

The main step in the implementation of the *DNL* methodology is the splitting of the wave field into "forward modes" and "backward modes", by means of the factorization of the polynomial bundle of order 2 defined in Eq. (3), which roots are founded by means of the solution of N_{lay} quadratic equations, by consequence, the planar *DNL* matrix is computed efficiently with a significant reduction of the computational cost.

In the planar case the computation the *DNL* matrix is exact at the discrete level. A small additional memory storage is required because the matrix *DNL* is a dense matrix, and it is incorporated to the coefficient matrix of the resulting linear equations system at the global level.

The performance of circular *DNL* method to solve Helmholtz equation in circular coordinates (r,θ) is very dependent of the propagation of the numerical errors at each layer, because the coefficients at the discrete Laplace operator are variables at the interior of the elements.

An important aspect in the implementation of circular *DNL* boundary condition is the accuracy determination of the localization of the far boundary ($r=r_e$) during the condensation process (see Fig. 2 (right)). It is known that the reflection coefficient in the far-field decreases as r_e value increases.

Now, we examine the influence of the localization from the far boundary r_e in the condensation process, with respect to the Medium Quadratic Error (E_2) given by the relation

$$E_2=\sqrt{\frac{1}{N_{lay}}\sum_{l=1}^{N_{lay}}|\phi_l^{j+1}-F^j\phi_l^j|^2} \tag{25}$$

where ϕ_l^j is given by

$$\phi_l^j=H_l^{(1)}(kr^j)\exp(i\theta_l)$$

Fig. 7 displays the Maximum Error E_2 for several kr_e values and an incident wave of length λ. We can appreciate that the Maximum Error decreases at the far-field as the kr_e values increases, and, at the same manner, the Maximum Error decreases at the near-field until a limit value of 0.025, thus, we can notice that the marching method is not stable, and the precision is worse at the near-field.

In this paper two strategies to improve the precision of DNL method are presented. Firstly, including a residual term in the transmission relation that allows us to collect the numerical errors from the condensation process. Secondly, using piecewise second order basis functions system at the main propagation direction a numerical difference scheme of fourth order is derived and thus, a transmission relation of two-layers is obtained.

2.3.3. Residual DNL method with one layer (RDNL1)

Consider the non-homogeneous transmission relation

$$(\phi^+)^{j+1}=\mathbf{F}^j(\phi^+)^j+\mathbf{R}^j \tag{26}$$

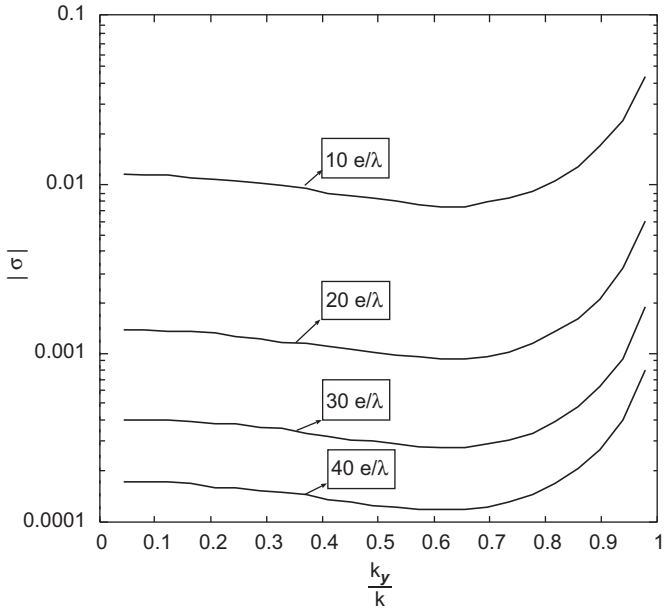

Fig. 6. Phase errors of the *DNL* boundary condition on uniform meshes.

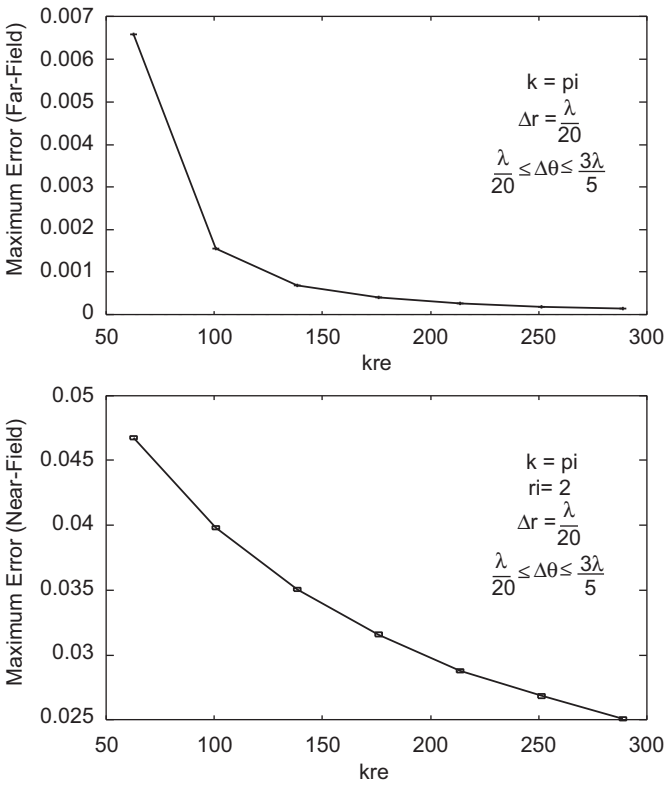

Fig. 7. Maximum Mean Quadratic Error due to *DNL* boundary condition. (Top) Maximum Mean Quadratic Error in the far-field. (Bottom) Maximum Mean Quadratic Error in the near-field.

where $\mathbf{R}^j$ vector is the source term relative to the j-layer. Substituting this relation into Eq. (2) are obtained the following formulas:

$$\mathbf{F}^{j-1} = -(\mathbf{A}^j\mathbf{F}^j + \mathbf{B}^j)^{-1}\mathbf{C}^j \tag{27}$$

$$\mathbf{R}^{j-1} = -(\mathbf{A}^j\mathbf{F}^j + \mathbf{B}^j)^{-1}\mathbf{A}^j\mathbf{R}^j \tag{28}$$

The second formula is new in the framework of the condensation process, and it allows us to calculate the numerical errors at each j-layer. Applying recursively these formulas from the far-field to the near-field is obtained the circular DNL with the corrector term at the near-field. Then, the formula (4) adopts the new form

$$(\phi^+)^2 = \mathbf{F}^1(\phi^+)^1 + \mathbf{R}^1 \tag{29}$$

at the near-field. To implement this recursive process we calculate the initial value vector $\mathbf{R}^M$, at the far-field, by means of the expression

$$\mathbf{R}^M = \phi^{M+1} - F^M\phi^M \tag{30}$$

where ϕ^M and ϕ^{M+1} are evaluated for each transversal mode $l = 1,2,\ldots,N_{lay}$ using the asymptotic expression of the analytical solution of the Helmholtz equation in circular coordinates (Tijonov and Samarsky, 1980)

$$\phi_l^j = \frac{\exp(i(kr^j + \theta_l))}{\sqrt{r^j}} \quad (j \geq M)$$

2.3.4. Two-layers DNL method (DNL2)

To achieve a higher precision of the numerical solution at the near-field a non-local homogeneous transmission relation with two layers is proposed to close the computational domain at the artificial boundary

$$(\phi^+)^{j+1} - \mathbf{F}^j(\phi^+)^j - \mathbf{G}^j(\phi^+)^{j-1} = 0 \tag{31}$$

where the $\mathbf{F}^j$ and $\mathbf{G}^j$ matrices are N_{lay} order matrices relative to j-layer. Using a piecewise quadratic basis functions system at the main direction to infinity, a higher order difference scheme is derived, and then, the second order discrete equations system (2) is replaced by the discrete equations system of fourth order

$$\mathbf{E}^j\phi^{j-2} + \mathbf{D}^j\phi^{j-1} + \mathbf{C}^j\phi^j + \mathbf{B}^j\phi^{j+1} + \mathbf{A}^j\phi^{j+2} = 0 \tag{32}$$

corresponding to the j-layer of the discretization. Putting

$$\phi^{j+s} = \mu^s\phi^j, \quad s = -2,-1,0,1,2 \tag{33}$$

and after some manipulations, we obtain the polynomial bundle of order 4

$$\mathbf{L}(\mu) = \mathbf{A}^j\mu^4 + \mathbf{B}^j\mu^3 + \mathbf{C}^j\mu^2 + \mathbf{D}^j\mu^1 + \mathbf{E}^j \tag{34}$$

An expression linearized from this bundle may be given by

$$\mathcal{L}(\boldsymbol{\mu}) = \mathcal{A}_0 - \boldsymbol{\mu}\mathcal{A}_1 \tag{35}$$

where

$$\mathcal{A}_0 = \begin{bmatrix} \mathbf{0} & \mathbf{I} & \cdots & \mathbf{0} \\ & \cdots & \ddots & \\ \mathbf{0} & \cdots & \mathbf{0} & \mathbf{I} \\ -\mathbf{E}^j & -\mathbf{D}^j & -\mathbf{C}^j & -\mathbf{B}^j \end{bmatrix} \mathcal{A}_1 = \begin{bmatrix} \mathbf{I} & \cdots & \cdots & \mathbf{0} \\ \vdots & \mathbf{I} & \ddots & \vdots \\ \vdots & \ddots & \mathbf{I} & \mathbf{0} \\ \mathbf{0} & \cdots & \mathbf{0} & \mathbf{A}^j \end{bmatrix}$$

If there is $\mathcal{A}_1^{-1}$ matrix, then we solve the eigenvalue problem

$$[\mathcal{A} - \mu\mathbf{I}]\Phi = 0$$

where $\mathcal{A} = \mathcal{A}_1^{-1}\mathcal{A}_0$, and

$$\mathcal{A} = \mathbf{V}\boldsymbol{\Lambda}\mathbf{V}^{-1}$$

where $\mathbf{V}$ is the eigenvector matrix of dimension $(4N_{lay})^2$ and

$$\boldsymbol{\Lambda} = diag(\mu_1,\mu_2,\ldots,\mu_{4N_{lay}})$$

is the diagonal matrix composed by the eigenvalues sequence $\mu_1,\mu_2,\ldots,\mu_{4N_{lay}}$. If the eigenvalues sequence $\mu_1,\mu_2,\ldots,\mu_{4N_{lay}}$ are roots from the polynomial $\mathbf{L}(\mu)$, then

$$\mathcal{A}(\mu)\mathbf{W} = \mathbf{W}\boldsymbol{\Lambda} \tag{36}$$

where $\mathbf{V} = \mathbf{W}$ is the Vandermonde matrix of order $4N_{lay}$. Based on it, Eq. (34) can be written as follows:

$$\begin{bmatrix} \mathcal{L}(\mu^+) & \mathcal{L}(\mu^-) \\ \mu^+\mathcal{L}(\mu^+) & \mu^-\mathcal{L}(\mu^-) \end{bmatrix} \begin{bmatrix} \phi^+ \\ \phi^- \end{bmatrix} = 0 \tag{37}$$

and the coefficient matrix determinant takes value zero

$$(\mu^+ - \mu^-)\mathcal{L}(\mu^+) = (\mu^+ - \mu^-)\mathcal{L}(\mu^-) = 0 \tag{38}$$

Using the eigenvalue decomposition (36), $\mathcal{L}(\mu^+)$ can be written as the form

$$\mathcal{L}(\mu^+) = \mathbf{W}^+[diag(\mu_1^+,\mu_2^+,\mu_3^+,\ldots,\mu_{2N_{lay}}^+)]\mathbf{W}^{+-1} \tag{39}$$

if Ker $\mathbf{W}^+ = 0$. Eqs. (36)–(38) reflect that the polynomial bundle (34) can be decomposed in two polynomial bundles of second order $\mathbf{P}(\mu^+)$ and $\mathbf{Q}(\mu^-)$, where $\mathbf{P}(\mu^+)$ collects the eigenvalues of $\mathcal{L}(\mu^+)$ and it can be given as the form

$$\mathbf{P}(\mu^+) = \mathbf{I}(\mu^+)^2 - \mathbf{F}^j(\mu^+)^1 - \mathbf{G}^j = 0 \tag{40}$$

being $\mathbf{F}^j$ and $\mathbf{G}^j$ matrices of order N_{lay}. Selecting adequately the eigenvalues of the eigenvalues sequence $\mu_1^+,\mu_2^+,\mu_3^+,\ldots,\mu_{2N_{lay}}^+$, the characteristic polynomial can be expressed as the following manner:

$$\prod_{l=1}^{N_{lay}}(\mu^+ - \mu_l^+)(\mu^+ - \mu_{(N_{lay}+l)}^+) = \prod_{l=1}^{N_{lay}}((\mu^+)^2 - \lambda_l^{sum}(\mu^+) + \lambda_l^{prod}) \tag{41}$$

where

$$\lambda_l^{sum} = \mu_l^+ + \mu_{N_{lay}+l}^+ \tag{42}$$

$$\lambda_l^{prod} = \mu_l^+\mu_{N_{lay}+l}^+ \tag{43}$$

for $l = 1,2,\ldots,N_{lay}$. Considering the diagonal matrices

$$\Lambda^{sum} = diag(\lambda_1^{sum},\lambda_2^{sum},\ldots,\lambda_{N_{lay}}^{sum}) \tag{44}$$

$$\Lambda^{prod} = diag(\lambda_1^{prod},\lambda_2^{prod},\ldots,\lambda_{N_{lay}}^{prod}) \tag{45}$$

the $\mathbf{F}^j$ and $\mathbf{G}^j$ matrices can be built as

$$\mathbf{F}^j = V\Lambda^{sum}V^{-1} \tag{46}$$

$$\mathbf{G}^j = -V\Lambda^{prod}V^{-1} \tag{47}$$

where V is a N_{lay} order matrix, which entries are chosen from the W^+ matrix, adequately. Using the relation (33) for $s = -1$, 0, 1 a discrete equation with two layers like (31) is obtained, and it is rewritten as

$$(\phi^+)^{j+1} = \mathbf{F}^j(\phi^+)^j + \mathbf{G}^j(\phi^+)^{j-1} \tag{48}$$

This new relation is a straightforward extension of DNL method to two layers, in case of the $\mathbf{F}^j$ and $\mathbf{G}^j$ matrices have N_{lay} eigenvalues, respectively. For this, an efficient procedure can be implemented to get the eigenvalues sequence $\mu_1^+,\mu_2^+,\mu_3^+,\ldots,\mu_{2N_{lay}}^+$ by means of the solution of N_{lay} equations of fourth degree analytically, where the coefficients of each fourth degree equation are the eigenvalues of matrices $\mathbf{E}^j,\mathbf{A}^j,\mathbf{B}^j,\mathbf{C}^j$ and $\mathbf{D}^j$, taken row by row, respectively.

2.3.5. Simulation of water waves problem with a DNL methodology

In this section we describe the main aspects of the *DNL* methodology taken into account to solve refraction–diffraction water waves problems governed by the Berkhoff equation (1). This methodology is based on the application of the numerical methods to solve the Berkhoff equation (1) on an unbounded domain. Fig. 8 shows various unbounded domains relative to refraction–diffraction problems mentioned above.

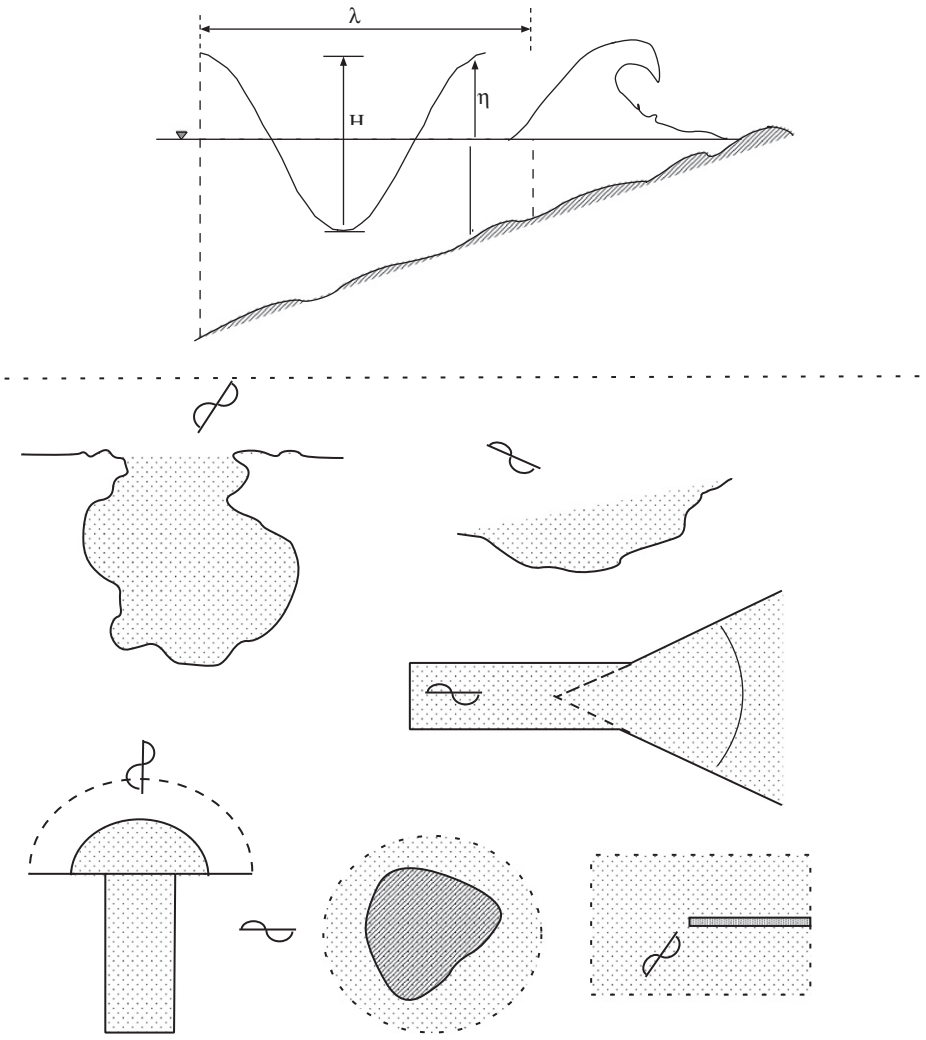

Fig. 8. Refraction–diffraction water waves problems in an unbounded domains.

On an unbounded domain an open boundary is selected to close the computational domain, and the outer part of it is a semi-infinite region, as can see in Fig. 9.

The implementation of the *DNL* method can be done taking into account the following steps:

(1) Identify the geometry and the computational domain.
(2) Discretize the computational domain.
(3) Identify the open boundary and the behaviour of the physical properties along the open boundary.
(4) Identify the shape of the unbounded domain corresponding to the physical problem.
(5) Design a patch of quadrilateral elements close to the computational domain, in the semi-infinite region (see Fig. 9)

- Rectangular channel (see Fig. 1).
- Island in the open sea or Harbour (see Fig. 2).

(6) Get the global matrices at the far-field, using

(a) linear shape function:

$\mathbf{A}^j, \mathbf{B}^j$ and $\mathbf{C}^j$

where in the homogeneous case for an uniform mesh, we get

$$\mathbf{A}^j = \left(\frac{1}{6}(kh)^2 + 1\right)\mathbf{I} - \frac{1}{6}\mathbf{M}^{-1}\mathbf{K}$$

$$\mathbf{B}^j = \left(\frac{2}{3}(kh)^2 - 2\right)\mathbf{I} - \frac{2}{3}\mathbf{M}^{-1}\mathbf{K}$$

$$\mathbf{C}^j = \left(\frac{1}{6}(kh)^2 + 1\right)\mathbf{I} - \frac{1}{6}\mathbf{M}^{-1}\mathbf{K}$$

(b) quadratic shape function:

$\mathbf{E}^j, \mathbf{A}^j, \mathbf{B}^j, \mathbf{C}^j$ and $\mathbf{D}^j$

where in the homogeneous case for an uniform mesh, we get

$$\mathbf{E}^j = -\left(\frac{1}{15}(kh)^2 + \frac{1}{6}\right)\mathbf{I} + \frac{1}{15}\mathbf{M}^{-1}\mathbf{K}$$

$$\mathbf{A}^j = \left(\frac{4}{15}(kh)^2 + \frac{8}{3}\right)\mathbf{I} - \frac{4}{15}\mathbf{M}^{-1}\mathbf{K}$$

$$\mathbf{B}^j = \left(\frac{24}{15}(kh)^2 - 5\right)\mathbf{I} - \frac{24}{15}\mathbf{M}^{-1}\mathbf{K}$$

These matrices are obtained integrating the Berkhoff equation (1) along the open boundary at the first time, and at the normal direction to the open boundary, at the second

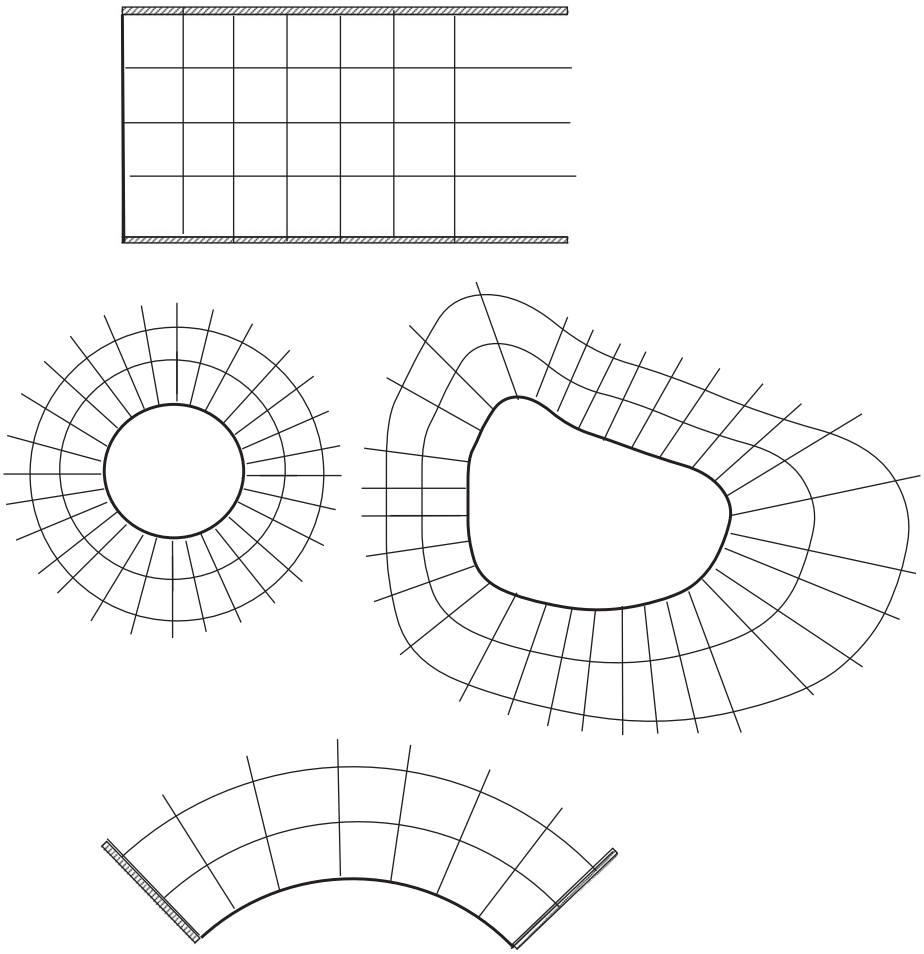

Fig. 9. Semi-infinite region with an open boundary selected with a dark line.

time. **M** and **K** are the mass and rigidez matrices along the open boundary direction, respectively.

(7) Get the *DNL* matrix at the near-field

(a) Direct method. This method is applied in case of the wave number k is constant at the unbounded domain, and the global matrices above mentioned are the same, for each j-layer in the discretization

(i) linear shape function: $(\phi^+)^{j+1}=\mathbf{F}^j(\phi^+)^j$ (see Eqs. (2)–(4));
(ii) quadratic shape function: $(\phi^+)^{j+1}=\mathbf{F}^j(\phi^+)^j+\mathbf{G}^j(\phi^+)^{j-1}$ (see Eqs. (32)–(48)).

The matrix **F** and **G** are obtained by solving the matricial equations. Using the linear shape functions is needed to solve Eq. (3), and using quadratic shape functions is need to solve Eq. (34). Both equations can be solve using Matlab.

(b) Iterative method using linear shape functions. This method is applied in case of the wave number k is variable at the unbounded domain and the global matrices above mentioned are dependent of the distance to the open boundary. Initial approximations of the matrices $\mathbf{F}^M$ and $\mathbf{R}^M$ are computed using Eqs. (2) and (30), respectively

- *DNL* method using Eq. (5).
- Residual *DNL* method $(\phi^+)^2=\mathbf{F}^1(\phi^+)^1+\mathbf{R}^1$ (see Eq. (29)) (using Eqs. (26)–(30)).

(8) Incorporate the *DNL* matrices to the stiffness matrix at the global level, according to the order of the open boundary nodes in the mesh.

2.4. Numerical results

The methodology described above was applied to a number of wave problems involving diffraction and refraction. It was applied to problems for which analytical solutions or laboratory data were available.

2.4.1. Wave focusing behind an elliptic shoal

For the purpose of testing the model for waves propagating over an irregular bathymetry, we have chosen the Ito and Tanimoto (1972) experiment. Their experimental bathymetry consists of a circular shoal resting on a flat bottom. A monochromatic wavetrain propagates over the shoal, and wave focusing occurs behind the shoal. Due to the axisymmetry of the circular shoal, the wave focusing pattern behind the shoal should be independent of the angle of incidence, if the model predicts it 'correctly'. The geometry of Ito and Tanimoto experiment is shown in Fig. 10. The water depth on the flat bottom $h_1=0.15$ m, and the water depth in the shoal region are described by $h=h_2+0.15625*((x-1.2)^2+(y-1.2)^2)$, where $h_2=0.05$ m is the depth at the shoal crest. A monochromatic wavetrain with 0.0104 m wave height and 0.511 s period enters the domain with normal incidence. Numerical solutions to this severe

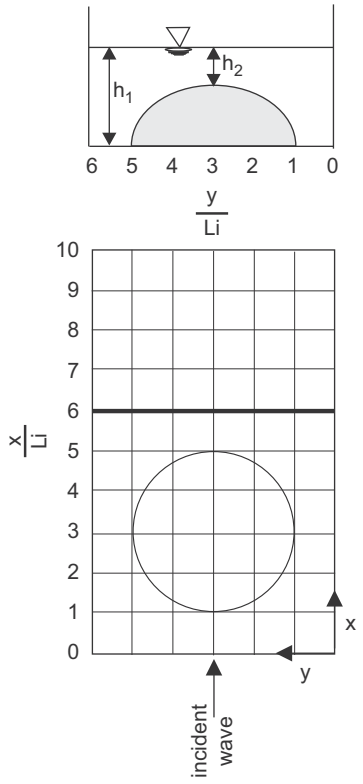

Fig. 10. Geometry of computational domain for the Ito and Tanimoto (1972) experiment.

test case have been given earlier (Berkhoff, 1976; Bettess and Zienkiewicz, 1977; Rivero et al., 1993; Kyung et al., 1990)

In this work, this problem has been resolved by finite elements in combination with the planar *DNL* boundary condition on the open boundary, located at the section $x/L_i = 6$. In contrast to the works above, this methodology reduces the computational cost drastically.

For the three different sections indicated in Fig. 11, a comparison between the model results with two different boundary conditions has been done. The absolute elevations on different sections are shown in Fig. 11. This figure shows that there are strong reflections when using first order local boundary condition in comparison to *DNL* planar boundary condition. The numerical results using *DNL* boundary condition reported here capture the maximum peak behind the shoal, in correspondence with the experimental results from Ito and Tanimoto (1972) reported in Kyung et al. (1990), in the case of $H_i/L_i = 0.0026$, being H_i and L_i the incident wave height and incident wavelength, respectively.

A further discussion relative to the behaviour of *DNL* boundary condition against the first order boundary condition in case of normal incidence is based on the calculus of mass flux through the open boundary. Integrating Eq. (1) in the computational domain labeled by Ω can be obtained the equation

$$\int_\Omega (\nabla_h (CC_g \nabla\phi) + k^2 CC_g \phi)\, d\Omega = \int_{\delta\Omega} CC_g \frac{\partial\phi}{\partial \mathbf{n}}\, d\sigma + \int_\Omega k^2 CC_g \phi\, d\Omega = 0 \tag{49}$$

where appear flux and mass integrals, respectively. An expression to compute the amount of mass in the computational domain is given by

$$\int_\Omega k^2 CC_g \phi\, d\Omega = -\int_{\delta\Omega} CC_g \frac{\partial\phi}{\partial \mathbf{n}}\, d\sigma \tag{50}$$

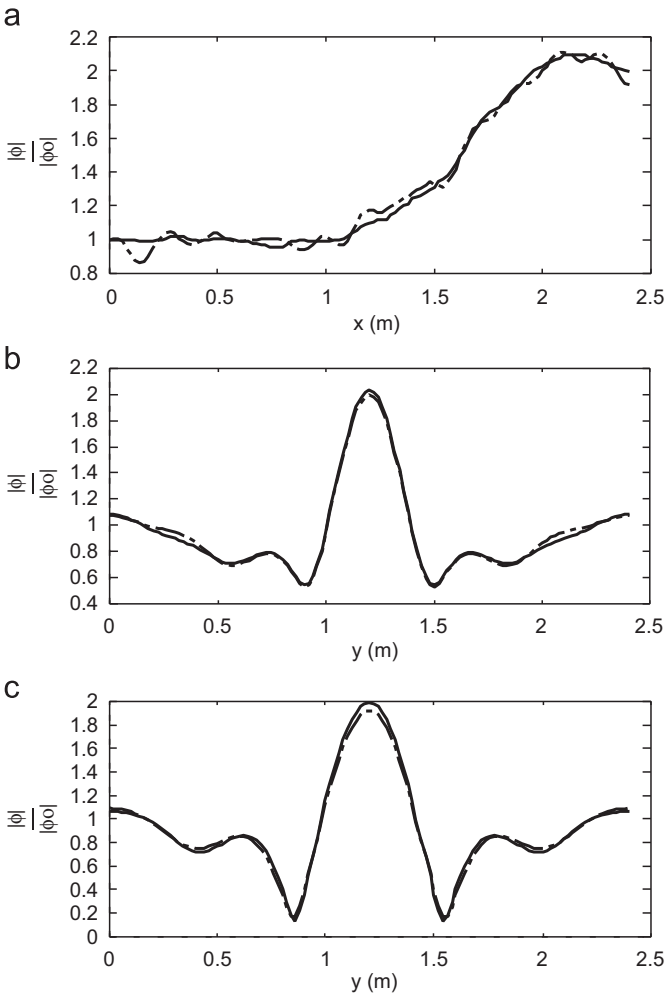

Fig. 11. (a) Section $y/L_i = 3$, (b) section $x/L_i = 5$, and (c) section $x/L_i = 6$. Comparison between the model results using boundary condition of first order, and the *DNL*, by means of normalized wave amplitudes with respect to the incident amplitude (–, DNL; – · · · –, boundary condition of first order).

and computing $\partial\phi/\partial\mathbf{n}$ explicitly we have the following formulas:

$$\int_\Omega k^2 CC_g \phi\, d\Omega = -\mathrm{i} \int_{\delta\Omega} kCC_g \phi\, d\sigma \tag{51}$$

corresponding to the first order local boundary condition, and

$$\int_\Omega k^2 CC_g \phi\, d\Omega = -\int_{\delta\Omega} CC_g \left[\frac{\partial\phi}{\partial \mathbf{n}}\right]_h d\sigma \tag{52}$$

corresponding to the *DNL* boundary condition, where $[\partial\phi/\partial\mathbf{n}]_h$ is computed numerically with the expression $[\partial\phi/\partial\mathbf{n}]_h = (\phi^{j+1} - \phi^j)/h$, h being the element size at the open boundary.

An indicator of the performance of an open boundary condition is the amount of mass that flux through by the open boundary goes to outer part of the computational domain, and by consequence, a boundary condition has better performance than other, if its mass computed is lower than ones.

Table 1 shows the mass computed with Eqs. (51) and (52) using four computational domains with an open boundary located approximately at the sections $x/L_i = 5$, 6, 7, 8, respectively. Numerical results are reported preserving the physical conditions above mentioned, and taken the real part of the mass integrals computed.

We can appreciate that the *DNL* boundary has better performance including if the open boundary is located at the section $x/L_i = 5$ very close to the shoal at the computational domain (see

Table 1
Comparison of the performance of open boundary conditions based on the outer mass flux. Mass computed for several domains with open boundary at the sections $x/L_i = 5, 6, 7, 8$.

Mass	$x/L_i = 5$	$x/L_i = 6$	$x/L_i = 7$	$x/L_i = 8$
First order	2.50974	1.44451	2.65784	2.65120
DNL	2.40558	1.03640	2.65655	2.63438

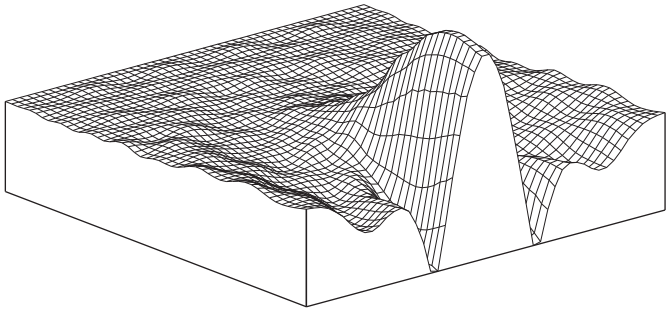

Fig. 12. Numerical results of the normalized amplitudes waves distribution. Perspective 3-D. Ito and Tanimoto (1972) experiment.

Fig. 10). Also, we can observe that the difference of mass fluxes is reduced as the open boundary is located far away from the shoal, as we can expected, while it is more noticeable for smaller computational domains, where the first order boundary condition is more reflecting and by consequence the mass increases.

Fig. 13(a) and (b) shows the normalized wave height along the central section $y/L_i = 2$ for two domains. The first domain closes with the artificial boundary located at the section $x/L_i = 5$, and the second is closed with the artificial boundary located at the section $x/L_i = 7$. In both cases the effect of smoothing due to the non-local property of the *DNL* is very significant in contrast to the oscilant behaviour of the first order local boundary condition. For the smallest domain, the prediction of the maximum peak is wrong, because it is not reached behind the shoal, according to the refraction theory.

The numerical results using the *DNL* boundary condition reported here show a good correspondence with the experimental results from Ito and Tanimoto (1972) and Kyung et al. (1990), in the case of $H_i/L_i = 0.0026$, H_i and L_i being the incident wave height and incident wavelength.

A plot of the wave height surface is shown in Fig. 12. In this figure, it is possible to appreciate the effect of the irregular bathymetry over the wave patterns. Behind the shoal the normalized wave height increases to 2.04.

2.4.2. Scattering of a plane wave by a circular island

The difference between an undisturbed wave and the field generated when the wave encounters an obstacle is called a scattered wave.

In the typical range of this phenomena the scattered wave usually does not destructively interfere with the incident wave, allowing their complete separation. As an example we have computed the scattering, by a circular island of radius a, of an incident plane wave travelling along the positive x-axis ($\theta = 0$) in a normal direction to the island's axis.

The analytical solution of the diffraction around a circular island has been given with the aid of a Bessel series expansion. Several numerical solutions of this kind of problem have been reported in Berkhoff (1976), Harari et al. (1998), and Bonet et al. (1997).

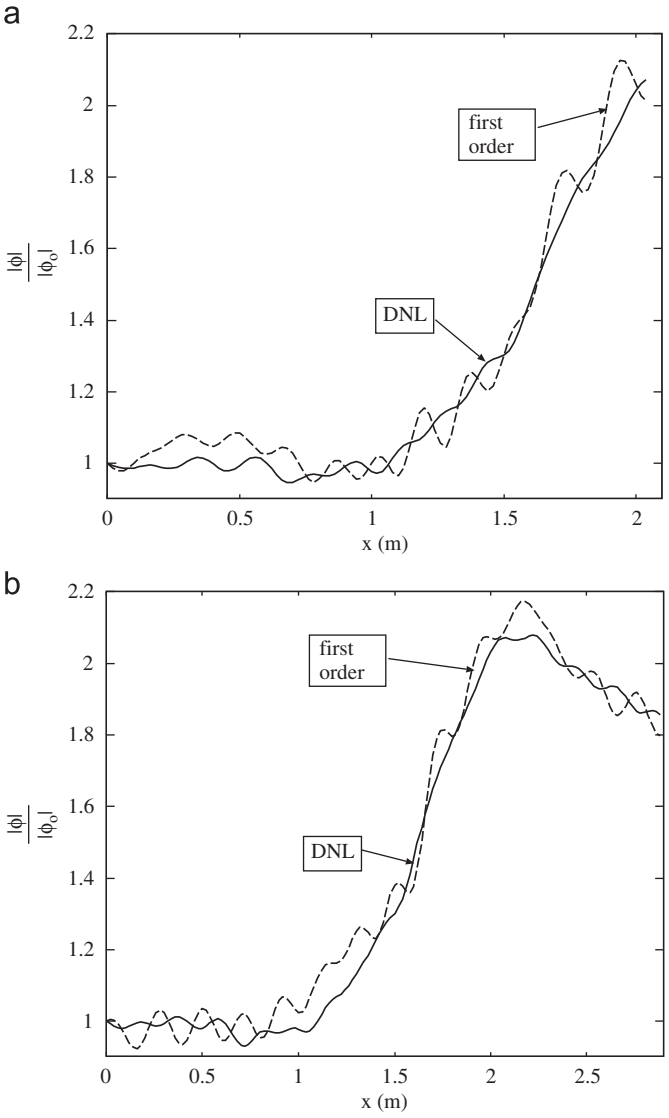

Fig. 13. Section $y/L_i = 1.2$. Comparison between the model results using a first order boundary condition, and the *DNL*: (a) Dominio computational with artificial boundary $x/L_i = 5$ and (b) Dominio computational with artificial boundary $x/L_i = 7$.

We have chosen a hard boundary on the wet surface to represent a rigid solid, and we have employed a condensation width of 8 wavelength.

Figs. 14 and 15 show the real/imaginary parts of the Galerkin solution, respectively, for different values of radius $R = a$, $1.4a$, and $2a$. In both figures, the numerical solutions represent the expected physical behavior of the solution. Fig. 16 shows absolute values of the analytical/numerical solution, respectively. Again, the excellent agreement between them is clear.

2.4.3. Diffraction for incident waves on an island located on a paraboloidal shoal

An island of cylindrical shape, located on a paraboloidal shoal in an infinite ocean of constant depth is attacked by long period plane incidence small amplitude regular waves (see Fig. 17).

The wave field around the island is calculated according to diffraction theory. The bathymetry for this case is shown in Fig. 17. This type of island is seemingly accepted as being representative for some real cases (Homma, 1950; Jonsson et al., 1976). In the shallow water approximation, the diffraction problem has

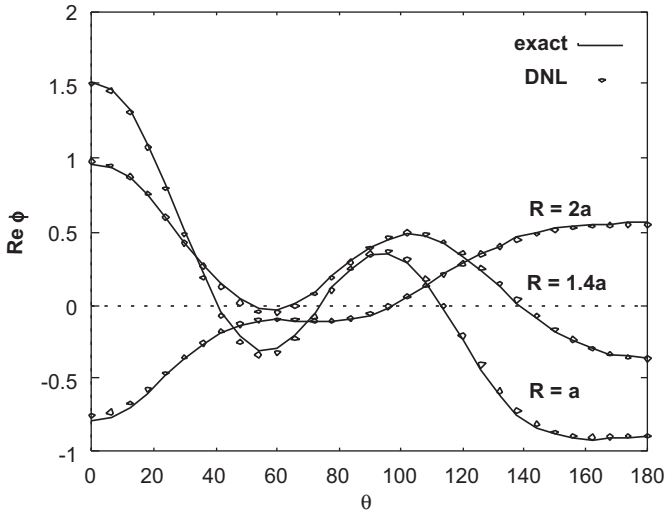

Fig. 14. Scattering of a plane wave (at $\theta=0$) by a circular island of radius a, $ka=\pi$. Real parts of the Galerkin solution at $R=a$, $1.4a$, $2a$.

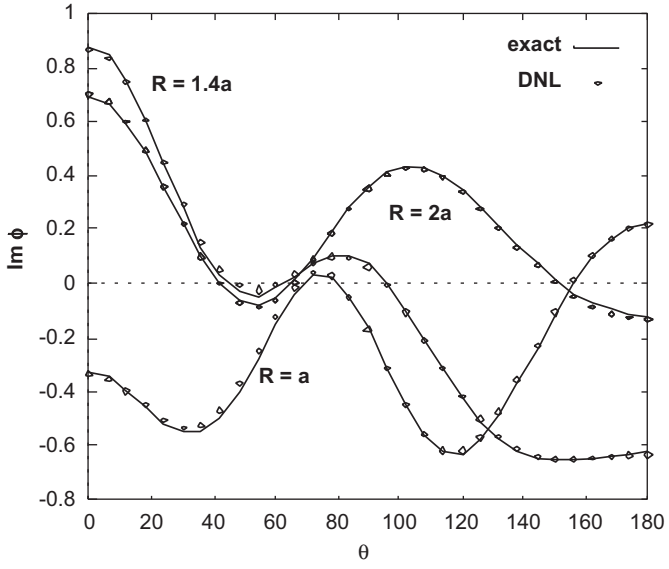

Fig. 15. Scattering of a plane wave (at $\theta=0$) by a circular island of radius a, $ka=\pi$. Imaginary parts of the Galerkin solution at $R=a$, $1.4a$, $2a$.

analytical solution and was reported in Homma (1950) solving an infinite set of linear two-point boundary problems.

The calculation of diffraction of water waves over a varying sea bed, based on finite element methods was reported (Berkhoff, 1976; Chen and Mei, 1974; Chen and Houston, 1987), initially. Chen and Mei used a Fourier–Bessel expansion as an exterior solution in a wave diffraction problem and used a specially devised variational statement to link the exterior solution with finite element solutions in the interior domain.

An important contribution on this way was the general methodology proposed for the solution of this problem using several strategies that allowed us to link finite element solutions to any kind of the Helmholtz equation exterior solution (analytical, series, or boundary integral) (Zienkiewicz, 1975; Zienkiewicz et al., 1977, 1978, 1979; Zienkiewicz and Bettess, 1976).

This problem has been also solved in Tsay and Liu (1983), Houston (1981), Bingyi et al. (1996), and Bonet et al. (1997). In the last reference, the author used the "sponge-filters" method to include in the numerical scheme the exact radiation condition at infinity.

The numerical solution by the finite element method+*DNL* procedure (Fig. 18) was obtained for the radius $r=r_e$ located 8λ from the artificial boundary. Fig. 18 depicts curves of relative amplitudes A/A_i at $r=r_a$, $r=2r_a$ and $r=3r_a$ vs. azimuth θ. The relative amplitudes at the shoreline (with a radius of $r_a=10$ km) correspond to the results reproduced in other papers (Homma, 1950; Houston, 1981) for a period of $T=240$ s. This curve has the same form as the curve obtained by Zienkiewicz et al. for this period, but, there is a discrepancy with the relative amplitudes reported by them, due to the difference in the geometrical parameters relative to the parabolic shoal. We note that for the same period, it causes an increased relative amplitude at the island increasing α. Fig. 19 shows the corresponding relative errors (%) at the island with a solid line. We can observe that the maximum relative errors diminish as the circle $r=r_e$ is placed far away from the computational domain.

3. Comparison *DNL* with local boundary conditions

Various boundary conditions on the artificial boundary will be numerically compared with the improved *DNLs* boundary conditions by considering the diffraction for incident waves on an island located on a paraboloidal shoal. Preserving the physical characteristics mentioned in the epigraph 2.4.3, we have used a mesh of 20 linear elements per wave on the annular region limited by

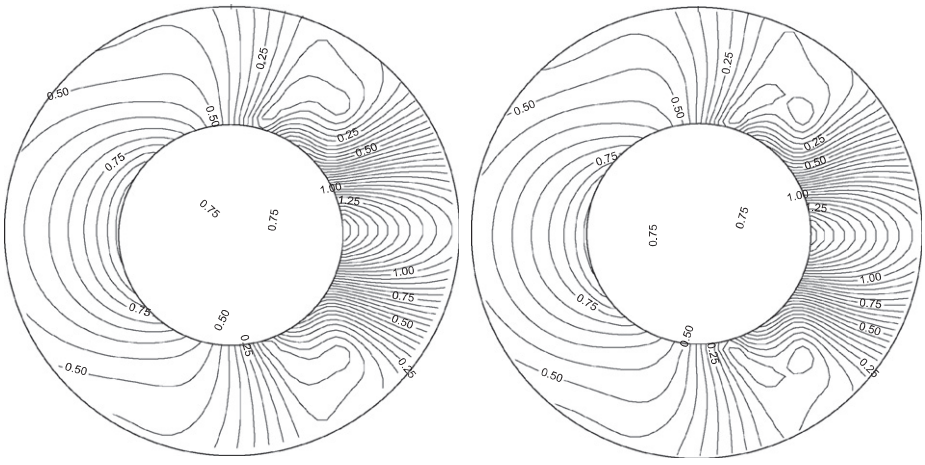

Fig. 16. Scattering of a plane wave (at $\theta=0$) by a circular island of radius a, $ka=\pi$. Absolute values of the nodal interpolation of the series solution (left) and the Galerkin solution (right).

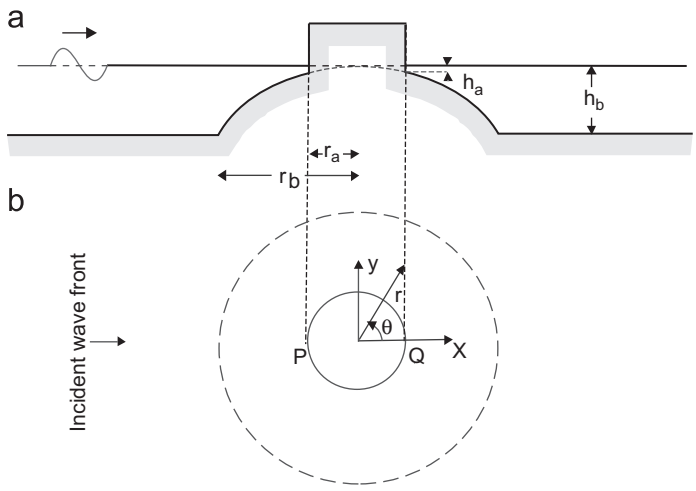

Fig. 17. Sketch of the idealized island on a paraboloidal shoal with $h=\alpha r^2$. (a) Vertical; $r_a=10$ km, $r_b=30$ km, $h_a=0.444$ km, $h_b=4$ km and (b) horizontal (after Jonsson et al., 1976).

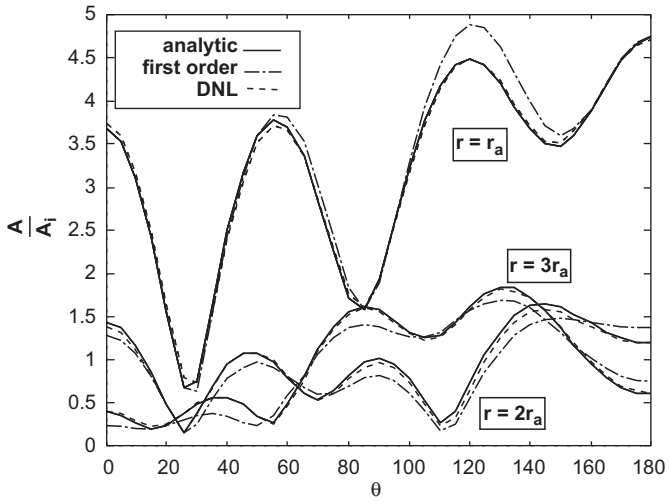

Fig. 18. Relative amplitude A/A_i vs. azimuth θ.

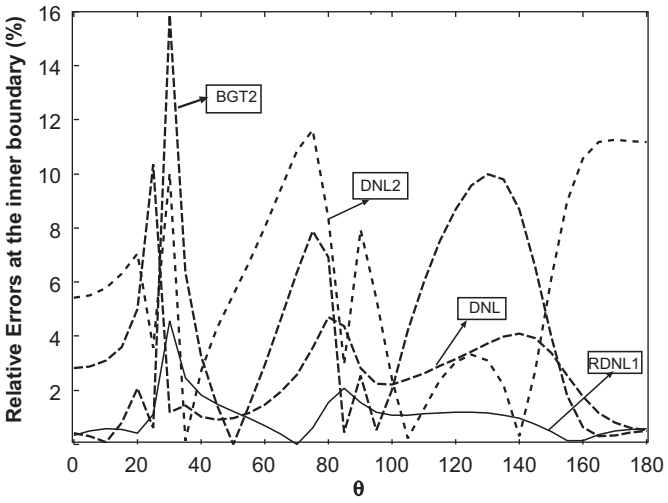

Fig. 20. (%) Relative errors at the inner boundary $r=r_a$ vs. azimuth θ.

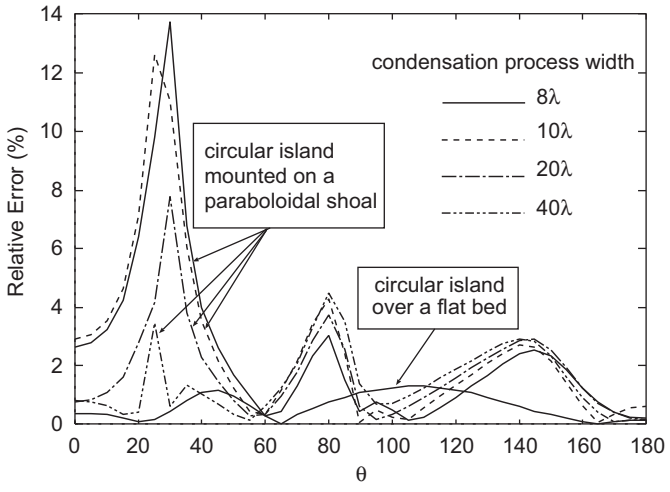

Fig. 19. Relative errors at shoreline vs. azimuth θ.

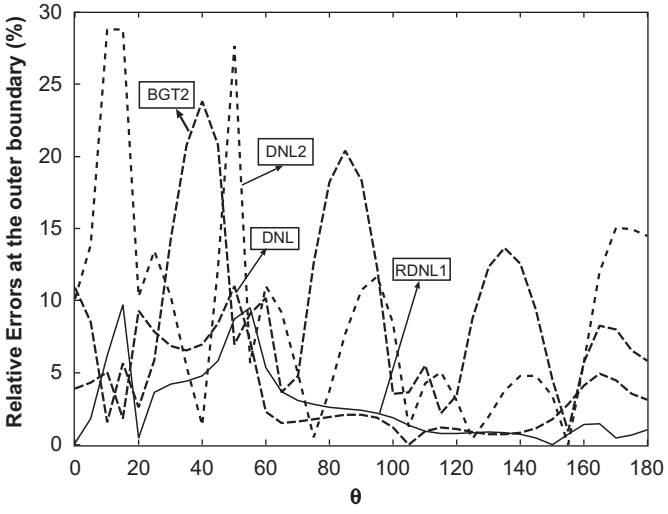

Fig. 21. (%) Relative errors at the outer boundary $r=r_b$ vs. azimuth θ.

$r_a \le r \le 3.21 r_a$. This discretization has been employing in all cases, taking linear shape functions at the transversal direction.

With the objective of an evaluation of the numerical performance of the proposed methodology, we compute the relative errors between the analytical solution and the numerical solutions on the inner boundary $r = r_a$. Fig. 20 shows the performance of the new class of absorbing boundary relative to known absorbing boundaries. In the figure can be noticed that *RDNL*1 reduces drastically the relative errors from the classical *DNL*, and of an uniform manner. Also can be observed that the *DNL*2 has a little better performance than a *BGT*2 absorbing boundary, in fact, it is according with expected behaviour, taking into account that the *DNL*2 is computed directly, without the application of the recursive process. The numerical results indicate a progress in the application of the *DNL* formulation to develop absorbing boundaries conditions to Helmholtz equation in anisotropic medium. Fig. 21 shows the relative errors (in %) at the outer boundary, and again the *RDNL*1 has the best performance.

4. Conclusions

The *DNL* methodology described above has been shown to be capable of solving diffraction and refraction water wave problems which extend to infinity, governed by Berkhoff equation. Extensions of the classical *DNL* method to *DNL*2 method and/or *RDNL*1 method allow us to improve its behaviour in case of significant variations of wave number in the domain. The *RDNL*1 method has the best performance reducing drastically the errors at the open boundary. In comparison with other main methods mentioned in the introduction the *DNL* methodology is generally enough for bi-dimensional unbounded problems. It is used in computational fluids by means of the solution relative to this problem, over a patch around the computational domain, using numerical scheme on a structured mesh. For rectangular geometry, the *DNL* method creates no reflection for incident monochromatic waves from an uniform unbounded medium. For circumferential geometry, this method causes a low reflection in the near field. This value diminishes when we locating r_e exterior radius from outer region away from the scatterers. In this process, the CPU time increases with the exterior radius r_e, without increasing the RAM memory. We recall that, in general, this kind of application is memory bounded. Furthermore, the number of operations can be drastically reduced by means of an eigenvalue decomposition of the matrix $M^{-1}K$. Also, this numerical procedure is applicable to domain decomposition problems using the non-local transference relations above derived. Future works are addresses to develop parallel algorithms for this problem, and to improve the behavior of *DNL* boundary operator to high dependence range of the refraction–diffraction index.

Acknowledgments

This work was supported by the Project of Faculty of Physics, Mathematics and Natural Sciences from National University of San Luis (Argentina) under the grant **PROICO** 22/F730O. We made extensive use of software distributed by GNU Fortran, the Free Software/GNU-Proyect:Linux ELF-OS, Octave, Tgif from William C. Cheng, and others. We also wish to thank the reviewers by their accurate comments and suggestions.

References

Berkhoff, J.C.W., 1976. Mathematical Models for Simple Harmonic Linear Water Waves: Wave Diffraction and Refraction. Tech. Rep. Public. Nro. 163, Delft Hydraulic Laboratory, Holland.

Bettess, P., Zienkiewicz, O.C., 1977. Diffraction and refraction of surface waves using finite and infinite elements. Int. J. Numer. Methods Eng. 11, 1271–1290.

Bingyi, X., Panchang, V.G., Demirbibek, Z., 1996. Exterior reflections in elliptic harbor wave models. J. Waterw. Port Coastal Ocean Eng. 122 (May), 118–126.

Bonet, R.P., Nigro, N., Storti, M.A., 1997. Solution of Berkhoff's equation with approximate radiation conditions. Rev. Int. Métodos Numér. Cálc. Dis Ing. 13 (4), 547–557.

Bonet, R.P., Nigro, N., Storti, M.A., Idelsohn, S.R., 1998. Condición absorbente discreta no-local (DNL) en diferencias finitas para modelos elípticos de propagación de ondas en el mar. Rev. Int. Métodos Numér. Cálc. Dis Ing. 14 (4), 481–500.

Bonet, R.P., Nigro, N., Storti, M.A., Idelsohn, S.R., 1999a. Condición absorbente discreta no-local (DNL) en elementos finitos para modelos elípticos de propagación de ondas en el mar. Rev. Int. Métodos Numér. Cálc. Dis Ing. 15 (1), 3–18.

Bonet, R.P., Nigro, N., Storti, M.A., Idelsohn, S.R., 1999b. Discrete non-local absorbing boundary condition for exterior problems governed by Helmholtz equation. Int. J. Numer. Methods Fluids 29, 605–621.

Chen, H.S., Houston, J.R., 1987. Calculation of Water Level Oscillation in Coastal Harbors. Report CERC 87-2, Coastal Engineering Research Center, WES, Vicksburg.

Chen, H.S., Mei, C.C., 1974. Oscillations and Wave Forces in an Offshore Harbor: Applications of Hybrid Finite Element Method to Water-wave Scattering. Report 190, Ralph M. Parsons Laboratory for Water Resources and Hydrodynamics, Mass. Inst. Tech.

Dasgupta, G., 1981. Sommerfeld radiation conditions and cloning algorithm, new concepts in finite element analysis. In: ASCE-ASME Summer Conference, vol. 44, New York, NY, pp. 47–66.

Givoli, D., 1991. Non-reflecting boundary conditions: a review. J. Comput. Phys. 94, 1–29.

Givoli, D., 1992a. A spatially exact non-reflecting boundary condition for time dependent problems. Comput. Methods Appl. Mech. Eng. 95, 97–113.

Givoli, D., 1992b. Numerical methods for problems. In: Infinite Domains in Studies in Applied Mechanics, vol. 33. Elsevier, Amsterdam.

Givoli, D., Keller, J.B., 1989. A finite element method for large domains. Comput. Methods Appl. Eng. 76, 41–66.

Harari, I., Hughes, T.J.R., 1994. Studies of domain-based formulations for computing exterior problems of acoustics. Int. J. Numer. Methods Eng. 37, 2935–2950.

Harari, I., Patlashenko, I., Givoli, D., 1998. Dirichlet-to-Neumann maps for unbounded wave guides. J. Comput. Phys. 143, 200–223.

Harari, I., Djellouli, R., 2004. Analytical study of the effect of wave number on the performance of local absorbing boundary conditions for acoustic scattering. Appl. Numer. Math. 50, 15–47.

Homma, S., 1950. On the behaviour of seismic sea waves around circular island. Geophys. Mag. 21, 199–208.

Houston, J.R., 1981. Combined refraction and diffraction of short waves using the finite element method. Appl. Ocean Res. 3, 163–170.

Ito, Y., Tanimoto, K., 1972. A method of numerical analysis of wave propagation. Application to wave diffraction and refraction. In: Proceedings of the 13th International Conference on Coastal Engineering, vol. 1. ASCE, Vancouver, Canada, pp. 503–522.

Jonsson, I.G., Skovgaard, O., Brink-Kjaer, O., 1976. Diffraction and refraction calculations for waves incident on an island. J. Mar. Res. 34 (3), 469–496.

Kyung, D.S., Dalrymple, R.A., Kirby, J.T., 1990. An angular spectrum model for propagation of stokes waves. J. Fluid Mech. 221, 205–232.

Rivero, F.J., Rodríguez, M.F., Arcilla, S.A., 1993. Propagación del oleaje sobre fondo variable y en presencia de corrientes. In: II Jornadas Esp. de Ing. de Costas y Puertos. Gijón, pp. 187–204.

Storti, M.A., D'Elía, J., Idelsohn, S.R., 1998. Algebraic discrete non-local (DNL) for the ship wave resistance problem. J. Comput. Phys. 146 (2), 570–602.

Thatcher, R.W., 1976. The use of infinite grid refinements at singularities in the solution of Laplace's equation. Numer. Math. 25, 163–178.

Thatcher, R.W., 1978. On the finite element method for unbounded regions. SIAM J. Numer. Anal. 15 (3), 456–477.

Tijonov, A.N., Samarsky, A.N., 1980. Ecuaciones de la Física Matemática. Editorial MIR. Moscú (in spanish).

Tsay, T.-K., Liu, P.L.-F., 1983. A finite element model for wave refraction and diffraction. Appl. Ocean Res. 5 (1), 30–37.

Wolf, J.P., Song, Ch., 1996. Finite Element Modelling of Unbounded Media. John Wiley & Sons, UK.

Zienkiewicz, O.C., 1975. The finite element method and boundary solution procedures as general approximation methods for field problems. In: World Congress on Finite Element Methods in Structural Mechanics. Bournemouth, pp. s1–s31.

Zienkiewicz, O.C., Bettess, P., 1976. Infinite elements in the study of fluid-structure interaction problems. In: The Second International Symposium on Computing Methods in Applied Science and Engineering, Versailles, France, pp. 133–172.

Zienkiewicz, O.C., Bettess, P., Kelly, D.W., 1978. The finite element method for determining fluid loading on rigid structures: two and three-dimensional formulations. In: Zienkiewicz, O.C., Lewis, R.W., Stagg, K.G. (Eds.), Numerical Methods in Offshore Engineering. Wiley, Chichester, pp. 141–183. (Chapter 4).

Zienkiewicz, O.C., Kelly, D.W., Bettess, P., 1977. The coupling of the finite element method and boundary solution procedures. Int. J. Numer. Methods Eng. 11 (2), 355–375.

Zienkiewicz, O.C., Kelly, D.W., Bettess, P., 1979. Marriage á la mode- or the best of both worlds. Boundary integrals and finite element procedures. In: Glowinski, R., Rodin, E.Y., Z.O.E. (Eds.), Energy Methods in Finite Element Analysis. Wiley, New York, pp. 81–106 (Chapter 5).